Journal of Sound and Vibration (2000) **235**(1), 133–151
doi:10.1006/jsvi.2000.2916, available online at http://www.idealibrary.com on IDEAL®

BIFURCATION BEHAVIOR OF A ROTOR SUPPORTED BY ACTIVE MAGNETIC BEARINGS

J. C. Ji

Theory of Lubrication and Bearing Institute, Xi'an Jiaotong University, Xi'an, Shaanxi 710049, *People's Republic of China*
Department of Building and Construction, City University of Hong Kong. E-mail: jchji2@hotmail.com

L. Yu

Theory of Lubrication and Bearing Institute, Xi'an Jiaotong University, Xi'an, Shaanxi 710049, *People's Republic of China*

AND

A. Y. T. Leung

Department of Building and Construction, City University of Hong Kong, Tat Chee Avenue, Kowloon, Hong Kong

(*Received* 6 *July* 1999, *and in final form* 19 *February* 2000)

The non-linear dynamics of a rigid rotor levitated by active magnetic bearings is investigated. The vibrations in the horizontal and vertical directions are analyzed on the center manifold near the double-zero degenerate point by using normal-form method. The resulting normal forms in the horizontal and vertical directions are different due to the effect of rotor weight. It is shown that the vibratory behavior in the vertical direction can be reduced on the center manifold to the Bogdanov–Takens form. For the autonomous case, there exist saddle-node bifurcation and Hopf bifurcation for local analysis, and a saddle-connection bifurcation for global analysis. For non-autonomous case, the Melnikov technique is used to determine the critical parameter at which the homoclinic orbits intersect transversally. For the vibrations in the horizontal direction, the essential non-linear terms of the truncated normal form are third order. The behaviors of zero solutions are given. Finally, numerical simulations are performed to verify the analytical predictions.

1. INTRODUCTION

Active magnetic bearings (AMBs) are now being widely used in rotating machinery. Most of the components of AMBs are non-linear therefore the entire system becomes inherently non-linear. The non-linear properties of AMBs can lead to a different behavior as predicted by a linear model. Several works have been done on the non-linear dynamical analysis of the rotor–AMB system, and many papers on AMB systems have been published on the bearing design, the bearing locations, the control strategy and the stability analysis. The non-linear oscillation caused by gyroscopic effects is analyzed in reference [1]. It is found that the system undergoes Hopf bifurcation to unstable periodic motions, and a non-linear feedback is used to control the Hopf bifurcation. The effects of co-ordinate coupling due to the geometric coupling of the pole arrangement on non-linear behavior are examined in

0022-460X/00/310133 + 19 $35.00/0

reference [2]. Multiple coexisting solutions and fractal boundaries are obtained. Stable quasiperiodic vibration is obtained for large geometic coupling values while neglecting the rotor weight in reference [3]. The collocation method is used to find both stable and unstable periodic solutions for geometric coupling with the rotor weight considered in reference [4]. The local stability and bifurcation behavior of the periodic motion are obtained by using Floquet theory.

It is important to note that, in most previous work, many authors considered their systems to have been stabilized by feedback control. The values of controller's gains are assumed to be far from critical. The current control principle is usually used for the sake of simplicity. In many situations, such an analysis can provide valuable information for dynamical behavior. However, some important information is lost in those systems under some special values of controller's gains. If the controller's gains are chosen in the neighborhood of some critical values, the system can exhibit more complicated behavior. Thus, the main objective of this paper is to provide a deeper insight into the effects of the critical values of controller's gains on the dynamic behavior of a magnetically suspended rotor. It will be shown that, due to the non-linear characteristics of magnetic forces, this system exhibits rich dynamics near the double-zero degenerate point and the controller's gains must be selected carefully.

There has been little research on codimension bifurcation of rotor motion. However, some applicable research has been conducted in bifurcation analysis for three-dimensional system. Holmes [5] studied the dynamics of a non-linear oscillator with a simple feedback system by using central manifold and normal form methods. Ge and Chen [6] analyzed double degeneracy and chaos in a rate gyro with feedback control. Tseng and Tung [7] investigated local bifurcations of codimension two for a flexible beam with active non-linear magnetic force via center manifold theory and the method of normal form theory. The actual magnetic force was approximated by a Taylor expanding about the equilibrium point keeping the lowest-order non-linear terms. The effects of feedback gains on the behavior of transverse vibrations of the beam and the region of attraction were obtained.

The present work examines the bifurcation behavior of a rotor–AMB system with critical feedback gains near the double-zero degenerate point. The voltage control strategy is used to take account for the effect of the inductance of bearing magnet. The normal form method, center manifold theory, and the Melnikov's technique are used to study local codimension two bifurcation of rotor motion. Finally, numerical simulations are also presented to verify the analytical results.

2. EQUATIONS OF MOTION

The rotor–AMB system under consideration is shown in Figure 1. A horizontal, uniform, symmetric, rigid rotor is suspended by two identical radial AMBs at both ends of the rotor. Each bearing is composed of four electromagnets, which are radially set opposite in the horizontal and vertical direction, respectively (see Figure 2). In order to simplify the analysis, the magnetic flux leakage, the flux fringing, the eddy current loss, the saturation of the core material, and the coupling effects between the electromagnets are neglected. The rotor is considered as a mass with two degrees of freedom. The equations of motion governing the unbalance response of the rotor can be written as

$$m\ddot{x} = F_x - c\dot{x} + me\omega^2 \sin \omega t,$$

$$m\ddot{y} = F_y - c\dot{y} + me\omega^2 \cos \omega t + mg, \tag{1}$$

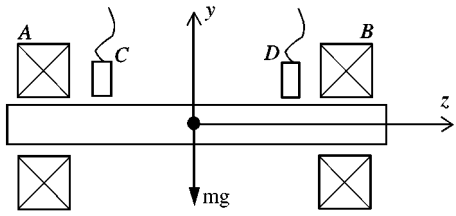

Figure 1. Model of a rigid rotor with active magnetic bearings (A, B) and sensors (C, D).

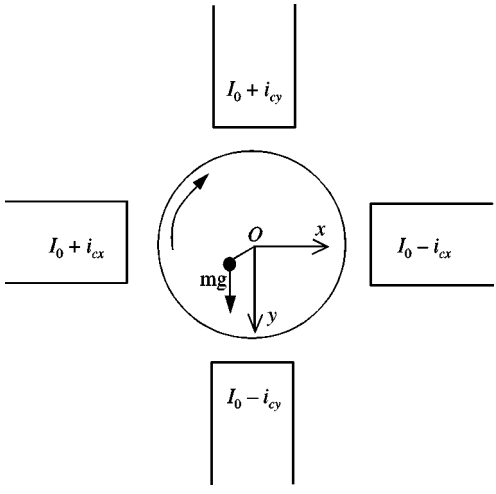

Figure 2. A simplified diagram for four assembled electromagnets.

where m, e, c, ω are the mass, the eccentricity of unbalance, the damping coefficient, and the regular velocity of the rotor respectively. F_x and F_y are the total magnetic forces in the horizontal and vertical directions respectively. Each of these forces is resulted from the difference of attractive forces of the two electromagnets. They take the forms [8]

$$F_x(i_{cx}, x) = -\frac{\mu_0 A_a N^2}{4}\cos\alpha\left[\left(\frac{I_0 + i_{cx}}{C_0 + x}\right)^2 - \left(\frac{I_0 - i_{cx}}{C_0 - x}\right)^2\right],$$

$$F_y(i_{cy}, y) = -\frac{\mu_0 A_a N^2}{4}\cos\alpha\left[\left(\frac{I_0 + i_{cy}}{C_0 + y}\right)^2 - \left(\frac{I_0 - i_{cy}}{C_0 - y}\right)^2\right], \tag{2}$$

where μ_0, A_a and N represent the permeability, the projection area of magnetic pole and the number of coil windings respectively. 2α is the angle between both shoes of a magnet. C_0 is the air gap. I_0, i_{cx} and i_{cy} denote the bias current and the control currents in the x and y directions respectively. $i_{cy} = i_0 + i$, $i_{cx} = i$, and i_0 denotes the static component of the current flowing through the coils in the vertically located electromagnets. If the rotor is expected to levitate at the geometric center of bearings during normal operation, the static component of force F_y must balance the weight of the rotor.

Thus, the static component of control current i_0 in the vertically located electromagnets satisfies

$$F_y(i_0, 0) + mg = 0,$$

or

$$mg = \frac{\mu_0 A_a N^2}{4} \cos\alpha \left(\frac{4 I_0 i_0}{C_0^2}\right). \tag{3}$$

From equations (1)–(3), it can be seen that the equations of motion and the expressions of the magnetic forces in both horizontal and vertical directions are similar by setting $i_0 = 0$. So it is enough to analyze the vibratory behavior in the y direction when the effect of cross-coupling is neglected. The dynamics in the x direction can be easily obtained in the same way. In subsequent work, the equation of motion in the y direction is studied.

The relationship of the current i and the voltage of the magnetic coil ΔV is given by [9]

$$\Delta V = L \frac{\mathrm{d}i}{\mathrm{d}t} + K_v \frac{\mathrm{d}y}{\mathrm{d}t} + iR, \tag{4}$$

where R, L and K_v stand for the Ohmic resistance, the inductance and the induced voltage-velocity coefficient of the coil, respectively. The input of the system is the actuator voltage, and the output of the system is the position of the rotor. When PD feedback control is used, the input of the system ΔV (voltage control strategy) obeys

$$\Delta V = K_p y + K_d \frac{\mathrm{d}y}{\mathrm{d}t}, \tag{5}$$

where K_p and K_d are the proportional and differential constants, and in the present research, the controllers' PD gains for four pole-pairs are taken to be identical.

Introducing non-dimensional parameters $w_0 = i_0/I_0$, $w = i/I_0$ and $v = y/C_0$, and expanding the magnetic force in a Taylor series about (0, 0) point, one has

$$F_y(w, v) = -\alpha_2' + \alpha_1' v - \alpha' w - 3\alpha_2' v^2 + 2\alpha_2' wv + 2\alpha_1' v^3 - 3\alpha' v^2 w + \alpha' v w^2 + 0(4), \tag{6}$$

where $\alpha' = \mu_0 A_a N^2 I_0^2 \cos\alpha / C_0^2$, $\alpha_1' = \alpha'(1 + w_0^2)$, $\alpha_2' = \alpha' w_0$, and 0(4) denotes the terms of order four and higher.

Substituting equations (6) and (5) into equations (1) and (4) respectively and letting $t \to rt$ and $\omega \to \omega/r$, yields the non-dimensional forms

$$\ddot{v} + \delta\dot{v} - \alpha_1 v + \alpha w + 3\alpha_2 v^2 - 2\alpha_2 wv - 2\alpha_1 v^3 + 3\alpha v^2 w - \alpha w^2 v = f\cos\omega t, \tag{7}$$

$$\dot{w} = k_1 v + k_2 \dot{v} - \beta w, \tag{8}$$

where $k_1 = (rC_0/I_0 L)K_p$, $k_2 = (C_0/I_0 L)(K_d - K_v)$, $\beta = rR/L$, $\delta = rc/m$, $\alpha = r^2\alpha'/mC_0$, $\alpha_1 = r^2\alpha_1'/mC_0$, $\alpha_2 = r^2\alpha_2'/mC_0$, $f = (r^2 e/C_0)\omega^2$ and $r^2 = C_0^2/(\mu_0 A_0 N^2 I_0^2 \cos\alpha)$.

Letting $(v, \dot{v}, \omega) = (x_1, x_2, x_3)$ and rewriting equations (7) and (8) yields a system of 3 first order equations

$$\dot{x}_1 = x_2,$$

$$\dot{x}_2 = \alpha_1 x_1 - \delta x_2 - \alpha x_3 - 3\alpha_2 x_1^2 + 2\alpha_2 x_1 x_3 + 2\alpha_1 x_1^3 - 3\alpha x_1^2 x_3 + \alpha x_1 x_3^2 + 0(4) + f\cos\omega t,$$

$$\dot{x}_3 = k_1 x_1 + k_2 x_2 - \beta x_3. \tag{9}$$

3. REDUCTION TO THE TRUNCATED NORMAL FORMS

In this section, the normal forms and unfoldings of a codimension-two bifurcation problem in the neighborhood of the double-zero-degenerate point are investigated. The corresponding autonomous system of equation (9) (by letting $f = 0$) has a static equilibrium point $(0, 0, 0)$. The Jacobian matrix of the linear part corresponding to equation (9) takes the form

$$A = \begin{bmatrix} 0 & 1 & 0 \\ \alpha_1 & -\delta & -\alpha \\ k_1 & k_2 & -\beta \end{bmatrix}. \tag{10}$$

According to the Routh–Hurwitz criterion [10], it is found that

(1) For $\alpha_1\beta/\alpha < k_1 < (\delta\beta(\delta + \beta) - \alpha_1\delta)/\alpha + (\delta + \beta)k_2)$, $k_2 > (1/\alpha)(\alpha_1 - \delta\beta)$: all the eigenvalues have negative parts, which implies the motion of the corresponding autonomous system of equation (9) is asymptotically stable at the fixed point.
(2) For $k_1 > \alpha_1\beta/\alpha$, $k_2 > (1/\alpha)(\alpha_1 - \delta\beta)$ and $k_1 = (\delta + \beta)k_2 + (1/\alpha)[(\delta\beta(\delta + \beta) - \alpha_1\delta)]$: a pair of eigenvalues becomes pure imaginary.
(3) For $k_1 = \alpha_1\beta/\alpha$, $k_2 > (1/\alpha)(\alpha_1 - \delta\beta)$: one zero-eigenvalue occurs.
(4) For $k_1 = k_{1c} = \alpha_1\beta/\alpha$, $k_2 = k_{2c} = (1/\alpha)(\alpha_1 - \delta\beta)$: there exist two zero-eigenvalue and a negative eigenvalue with the value of $-(\delta + \beta)$.

Figure 3 demonstrates the stability region of static equilibrium point and a criterion for the choice of feedback gains. If the controller's gains are selected in the region between curves "AB" and "AC", the motion of the linearized autonomous system is asymptotically stable at the origin. In a practical system, the controller's gains must be chosen in this region in order to stabilize the system. The other regime is unstable for the fixed point. There exists a pair of pure imaginary eigenvalues on curve AB and one zero eigenvalue on curve AC. These two curves are the stability boundary. The Hopf bifurcation occurs when the controller's parameters pass through curve AB, whereas saddle-node bifurcation occurs when pass through curve AC. These two cases are called local bifurcation of codimension one. Curves AB and AC meet at point A, where there is a double-zero eigenvalue.

In this work, special attention is paid to case (4), where the Jacobian matrix has a double zero and a negative eigenvalue. It is called codimension-two bifurcation problem. The main purpose is to find the loci in the parametric plane and to observe the qualitative behavior when the parameters are varied. By the center manifold theory [11], the study of the dynamics of the three-dimensional system (9) can be reduced to the corresponding

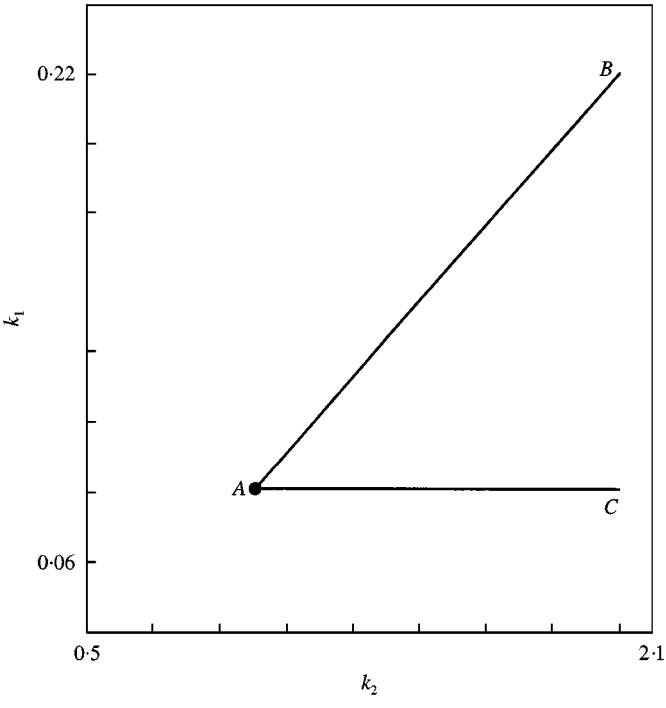

Figure 3. The parametric diagram for selection of controller's gains.

two-dimensional center manifold which determines the key qualitative dynamical behavior. To achieve this, introducing small perturbation ε_1 and ε_2 in the forms

$$k_1 = k_{1c} + \varepsilon_1, \quad k_2 = k_{2c} + \varepsilon_2, \tag{11}$$

so that the unfolding of the critical system ($\varepsilon_1 = \varepsilon_2 = 0{\cdot}0$) will be included in the parametrized normal form. The co-ordinate transformation $x = Tp$ yields the standard form of equation (9),

$$\dot{p} = [J]p + [J]_\varepsilon p + T^{-1}\begin{bmatrix} 0 \\ f(Tp) \\ 0 \end{bmatrix} + T^{-1}\begin{bmatrix} 0 \\ f(t) \\ 0 \end{bmatrix}, \tag{12}$$

where both the non-linear terms and the time-periodic perturbation terms are evaluated at the critical values, in which p, $[J]$, $[J]_\varepsilon$, T are given in Appendix A.

According to the center manifold theory, the center manifold will be given by $p_3 = h(p_1, p_2)$, i.e. $p_3 = 0(|p_i|^2)$ for the second order terms to determine the qualitative behavior near $(0,0,0)$ point, or $p_3 = h(p_1, p_2)$, i.e. $p_3 = 0(|p_i|^3)$ for the third order terms to control the qualitative behavior. Thus, the corresponding reduced system is

$$\begin{Bmatrix} \dot{p}_1 \\ \dot{p}_2 \end{Bmatrix} = \begin{bmatrix} 0 & 1 \\ 0 & 0 \end{bmatrix}\begin{Bmatrix} p_1 \\ p_2 \end{Bmatrix} + \begin{bmatrix} a_{11} & a_{12} \\ a_{21} & a_{22} \end{bmatrix}\begin{Bmatrix} p_1 \\ p_2 \end{Bmatrix} + \begin{Bmatrix} f'_{11} \\ f'_{12} \end{Bmatrix} + \begin{Bmatrix} f'_{21} \\ f'_{22} \end{Bmatrix} + \begin{bmatrix} C_1 f\cos\omega t \\ C_2 f\cos\omega t \end{bmatrix} + \text{h.o.t.}, \tag{13}$$

where

$$f'_{11} = C_1 b_{11} p_1^2 + C_1 b_{22} p_2^2 + C_1 b_{12} p_1 p_2,$$

$$f'_{12} = C_2 b_{11} p_1^2 + C_2 b_{22} p_2^2 + C_2 b_{12} p_1 p_2,$$

$$f'_{21} = C_1 b_{111} p_1^3 + C_1 b_{222} p_2^3 + C_1 b_{112} p_1^2 p_2 + C_1 b_{122} p_1 p_2^2,$$

$$f'_{22} = C_2 b_{111} p_1^3 + C_2 b_{222} p_2^3 + C_2 b_{112} p_1^2 p_2 + C_2 b_{122} p_1 p_2^2,$$

the h.o.t. denotes terms of orders $0(|p_i^5|)$, $0(|\varepsilon_i p_i^3|)$, and $0(|\varepsilon_i^2 p_i|)$, and the coefficients C_i, b_{ij}, b_{ijk} are defined in Appendix B. Although the computations of center manifold are confined to the autonomous form, here the excitation terms are treated as a small perturbation and computed in the same way [6]. In section 4, the effect of the excitation will be investigated by the Melnikov's method to detect the parameter values at which the homoclinic or heteroclinic orbits intersect transversally.
By using a linear change of co-ordinates

$$\begin{Bmatrix} p_1 \\ p_2 \end{Bmatrix} = \begin{bmatrix} 1 + a_{12} & 0 \\ -a_{11} & 1 \end{bmatrix} \begin{Bmatrix} q_1 \\ q_2 \end{Bmatrix}, \tag{14}$$

equation (13) becomes a more convenient form:

$$\begin{Bmatrix} \dot{q}_1 \\ \dot{q}_2 \end{Bmatrix} = \begin{bmatrix} 0 & 1 \\ \mu_1 & \mu_2 \end{bmatrix} \begin{Bmatrix} q_1 \\ q_2 \end{Bmatrix} + \begin{Bmatrix} f_{11} \\ f_{12} \end{Bmatrix} + \begin{Bmatrix} f_{21} \\ f_{22} \end{Bmatrix} + \begin{Bmatrix} C_1 f \cos \omega t \\ C_2 f \cos \omega t \end{Bmatrix} + \text{h.o.t.}, \tag{15}$$

where

$$f_{11} = C_1 b_{11} q_1^2 + C_1 b_{22} q_2^2 + C_1 b_{12} q_1 q_2,$$

$$f_{12} = C_2 b_{11} q_1^2 + C_2 b_{22} q_2^2 + C_2 b_{12} q_1 q_2,$$

$$f_{21} = C_1 b_{111} q_1^3 + C_1 b_{222} q_2^3 + C_1 b_{112} q_1^2 q_2 + C_1 b_{122} q_1 q_2^2,$$

$$f_{22} = C_2 b_{111} q_1^3 + C_2 b_{222} q_2^3 + C_2 b_{112} q_1^2 q_2 + C_2 b_{122} q_1 q_2^2,$$

$$\mu_1 = -\frac{\alpha \varepsilon_1}{\delta + \beta}, \; \mu_2 = \frac{\alpha}{(\delta + \beta)^2} \varepsilon_1 - \frac{\alpha}{\delta + \beta} \varepsilon_2.$$

At this stage, the method of normal forms is employed to simplify the reduced system in which the qualitative dynamics are still captured in the neighborhood of the fixed point. To achieve this, a near-identity co-ordinate transformation is chosen as

$$q = u + Poly\,2(u), \tag{16}$$

where the simple notation $Poly2(u)$ represents the polynomial terms of order 2. Thus, the truncated normal form (containing excitation terms) is given by

$$\dot{u}_1 = u_2 + f_1 \cos \omega t,$$

$$\dot{u}_2 = \mu_1 u_1 + \mu_2 u_2 + a_1 u_1^2 + b_1 u_1 u_2 + f_2 \cos \omega t, \tag{17}$$

where $a_1 = C_2 b_{11}$, $b_1 = 2C_1 b_{11} + C_2 b_{12}, f_1 = C_1 f$, $f_2 = C_2 f$. In this case, the quadratic coefficients b_{11}, b_{12}, b_{22} do not vanish, thus the terms of order 3 and higher can be neglected.

To put equation (17) into the Bogdanov–Takens form [11], letting $\bar{u}_1 = u_1 + \mu_1/2a_1$ and $\bar{u}_2 = u_2$, yields

$$\dot{\bar{u}}_1 = \bar{u}_2 + f_1 \cos \omega t,$$

$$\dot{\bar{u}}_2 = \bar{v}_1 + \bar{v}_2 \bar{u}_2 + a_1 \bar{u}_1^2 + b_1 \bar{u}_1 \bar{u}_2 + f_2 \cos \omega t, \tag{18}$$

where $\bar{v}_1 = -\mu_1^2/4a_1$ and $\bar{v}_2 = \mu_2 - (b_1/2a_1)\mu_1$.

Following the procedure outlined above, the truncated normal form for the dynamics in the x direction can easily be obtained by simply setting $\alpha_1 = \alpha$, $\alpha_2 = 0$ in equation (15) and noting the difference of excitation terms in equation (1) as follows:

$$\dot{u}_1 = u_2 + f_1 \sin \omega t,$$

$$\dot{u}_2 = \mu_1 u_1 + \mu_2 u_2 + a_2 u_1^3 + b_2 u_1^2 u_2 + f_2 \sin \omega t, \tag{19}$$

where $a_2 = C_2 b_{111}$, $b_2 = C_2 b_{112} + 3C_1 b_{111}, f_1 = C_1 f, f_2 = C_2 f$. Substituting coefficients b_{111} and b_{112} given in Appendix B into a_2 and b_2, and recalling the relationship $\alpha_1 = \alpha$, one finds that a_2 vanishes whereas b_2 does not vanish, thus terms of order four and higher can be neglected.

It is easy to see from equations (18) and (19) that the truncated normal forms for the two directions are different due to the effect of rotor weight. The necessary lowest order non-linear terms are third order for the horizontal direction and second order for the vertical direction respectively. The addition of higher order terms in equations (18) and (19) does not affect the qualitative behavior of the truncated system near (0, 0, 0). The dynamical behavior of the original system can be reduced on the center manifold near the critical degenerate system. In the subsequent work, the above forms will be used for the purpose of bifurcation analysis.

4. BIFURCATION OF ROTOR MOTION IN THE VERTICAL DIRECTION

With suitable rescaling to equation (18), the corresponding simple forms can be reduced to $a_1 = b_1 = 1$. To achieve this, letting $\bar{u}_1 = r_1 u_1$, $\bar{u}_2 = r_2 u_2$, $t \to r_3 t$ for system (18), yields

$$\dot{u}_1 = u_2 + \bar{f}_1 \cos(\Omega t),$$

$$\dot{u}_2 = v_1 + v_2 u_2 + u_1^2 + u_1 u_2 + \bar{f}_2 \cos(\Omega t), \tag{20}$$

where $r_1 = a_1/b_1^2$, $r_2 = a_1^2/b_1^3$, $r_3 = b_1/a_1$, $v_1 = (r_3/r_2)\bar{v}_1$, $v_2 = r_3 \bar{v}_2$, $\bar{f}_1 = (r_3/r_1) f_1$, $\bar{f}_2 = (r_3/r_2)\, f_2$, $\Omega = r_3 \omega$.

For bifurcation analysis, the corresponding autonomous system of equation (20) has been studied extensively. The unfolding results of references [11, 12] can be consequently employed to directly show the dynamical behavior of the full system on the center manifold near the double-zero-degenerate point.

4.1. THE QUALITATIVE BEHAVIOR FOR THE AUTONOMOUS CASE

The corresponding autonomous system of equation (20) is obtained by letting $f = 0$:

$$\dot{u}_1 = u_2,$$

$$\dot{u}_2 = v_1 + v_2 u_2 + u_1^2 + u_1 u_2. \tag{21}$$

Here the main results of system (21) are summarized as follows. First, the fixed points of the system are given by $(\pm\sqrt{-v_1}, 0)$, and hence only exist for $v_1 \leqslant 0$. By checking the linearized stability for these fixed points, it is easy to find that $(+\sqrt{-v_1}, 0)$ is a saddle for $v_1 < 0$ and all v_2, while $(-\sqrt{-v_1}, 0)$ is a source for $v_2 > -\sqrt{-v_1}$, $v_1 < 0$, and a sink for $v_2 < \sqrt{-v_1}$, $v_1 < 0$. Saddle-node bifurcations occur on $v_1 = 0$, $v_2 \neq 0$ while a subcritical Hopf bifurcation occurs on the curve $v_2 = \sqrt{-v_1}$.

In addition to the saddle-node bifurcation and Hopf bifurcation for local analyses, a saddle-connection bifurcation for global analysis is expected to occur. To study this, a rescaling transformation is introduced. Letting $u_1 \to \varepsilon^2 u_1$, $u_2 \to \varepsilon^3 u_2$, $v_1 \to \varepsilon^4 v_1$, $v_2 \to \varepsilon^2 v_2$, $t \to \varepsilon t$, so that equation (21) becomes

$$\begin{aligned} \dot{u}_1 &= u_2, \\ \dot{u}_2 &= v_1 + u_1^2 + \varepsilon(v_2 u_2 + u_1 u_2). \end{aligned} \tag{22}$$

For $\varepsilon = 0$, the system (22) becomes an integral Hamiltonian system with Hamiltonian function

$$H(u_1, u_2) = \frac{u_2^2}{2} - v_1 u_1 - \frac{u_1^3}{3}. \tag{23}$$

By applying the Melnikov technique, the autonomous system has an approximate homoclinic bifurcation curve by

$$v_1 = \left(-\frac{49}{25}\right) v_2^2, \quad v_2 \geqslant 0. \tag{24}$$

Figure 4 shows the bifurcation diagram and its associated phase portraits for system (21). The associated phase portraits are topologically equivalent to the flow on the center manifold.

4.2. THE MELNIKOV ANALYSIS

It has been seen that for the corresponding autonomous system there exists a saddle connection on $v_1 = (-49/25)\, v_2^2$, $v_2 \geqslant 0$, for equation (22). If the system has perturbations, i.e., $f \neq 0{\cdot}0$, this system becomes non-autonomous, and the homoclinic orbit may be broken. By applying Melnikov's technique, one can prove the existence of transverse homoclinic orbit in the system. Using the rescaling transformation $u_1 \to \varepsilon^2 u_1$, $u_2 \to \varepsilon^3 u_2$,

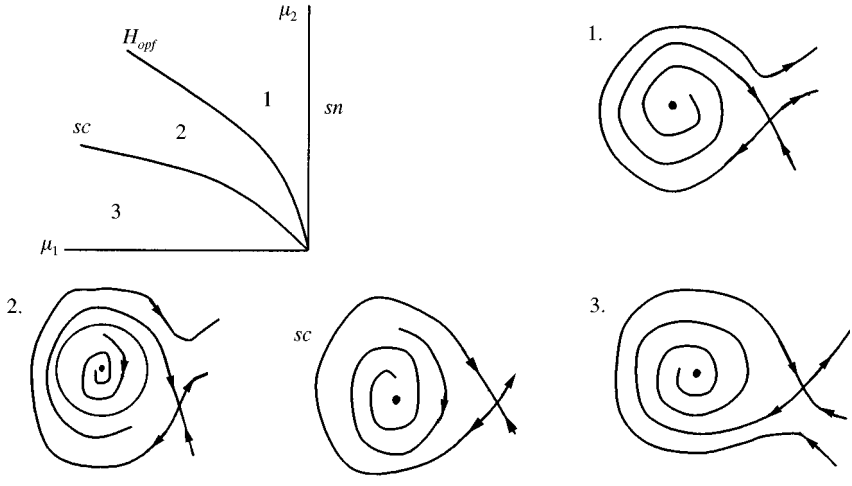

Figure 4. The complete bifurcation sets and its phase portraits of equation (23): "sn", saddle-node bifurcation; "Hopf', Hopf bifurcation; "sc", saddle connection bifurcation.

$v_1 \to \varepsilon^4 v_1,\ v_2 \to \varepsilon^2 v_2,\ t \to \varepsilon t,\ \bar{f}_1 = \varepsilon^5 f_1,\ \bar{f}_2 = \varepsilon^5 f_2$ and neglecting higher order terms of ε, equation (21) becomes

$$\begin{aligned} \dot{u}_1 &= u_2, \\ \dot{u}_2 &= v_1 + \varepsilon v_2 u_2 + u_1^2 + \varepsilon u_1 u_2 + \varepsilon f_2 \cos(\omega t), \end{aligned} \tag{25}$$

where $\omega = \varepsilon\Omega$. For $\varepsilon = 0$, equation (25) has a saddle connection orbit given by

$$(u_1^0(t),\, u_2^0(t)) = \left(\pm \left(1 - 3\,\mathrm{sech}^2\left(\frac{t}{\sqrt{2}}\right)\right), \pm 3\sqrt{2}\,\mathrm{sech}^2\left(\frac{t}{\sqrt{2}}\right)\tanh\left(\frac{t}{\sqrt{2}}\right)\right). \tag{26}$$

The Melnikov function for the homoclinic orbit (the computation is for " + " in equation (26), while for " − " is identical) is given by

$$M(t_0) = \int_{-\infty}^{+\infty} u_2^0(t)\left[v_2 u_2^0(t) + u_1^0(t) u_2^0(t) + f_2 \cos\left[\omega(t + t_0)\right]\right] \mathrm{d}t. \tag{27}$$

Substituting equation (26) into equation (27) gives

$$M(t_0) = \frac{12\sqrt{2}}{35}(7v_2 - 5) - \frac{3}{2}\pi\omega_1^2 f_2\,\mathrm{cosech}\frac{\pi\omega_1}{2}\sin(\omega_1 t_0) \tag{28}$$

where $\omega_1 = \sqrt{2}\omega$. Suppose that $M(t_0)$ has a simple zero, i.e., there exists a point $t_0 = \bar{t}_0$ such that

$$M(\bar{t}_0) = 0 \quad \text{and} \quad \frac{\partial M(\bar{t}_0)}{\partial t_0} \neq 0 \tag{29}$$

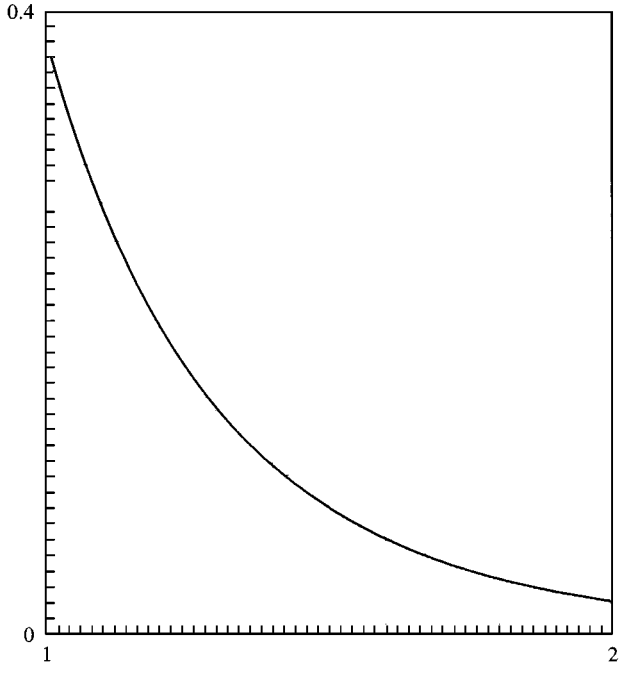

Figure 5. The Melnikov criterion in (ω_1, f_2) plane. The stable and unstable manifolds of a saddle-type periodic orbit may intersect transversely in the region above the curve.

then the stable and unstable perturbed manifolds that are close to homoclinic manifold of the unperturbed system intersect transversely, and there exist transverse homoclinic orbits at certain parameter values and some t_0. It follows from the Melnikov theory that if the forcing amplitude satisfies

$$f_2 > \frac{8\sqrt{2}}{35}(7v_2 - 5) \Big/ \left(\pi\omega_1^2 \operatorname{cosech} \frac{\pi\omega_1}{2}\right), \tag{30}$$

the manifolds of equation (25) intersect and may give rise to chaotic motions of the Smale-horseshoe type near the saddle point. Equation (30) is numerically computed at the specific values of controller's gains and system parameters and the result is shown in Figure 5. The stable and unstable manifolds of a saddle-type periodic orbit may intersect transversely in the region above the curve.

5. DYNAMIC BEHAVIOR IN THE HORIZONTAL DIRECTION

From the analysis in section 3, the reduced equation of motion in the horizontal direction can be written in the form (by letting $a_2 = 0$ in equation (19))

$$\begin{aligned} \dot{u}_1 &= u_2 + f_1 \sin \omega t, \\ \dot{u}_2 &= \mu_1 u_1 + \mu_2 u_2 + b_2 u_1^2 u_2 + f_2 \sin \omega t, \end{aligned} \tag{31}$$

where

$$\mu_1 = -\frac{\alpha\varepsilon_1}{\delta+\beta}, \quad \mu_2 = \frac{\alpha}{(\delta+\beta)^2}\varepsilon_1 - \frac{\alpha}{\delta+\beta}\varepsilon_2, \quad b_2 = \frac{\delta\beta}{\delta+\beta}.$$

Usually, by using the van der Pol transformation and applying the averaging method [11], equation (31) can become an averaged system and the bifurcation of fixed points occurring in the averaged system can be explored near resonance. But for this physical system, the trivial solution for the corresponding autonomous system of equation (31) is of significant interest because the rotor is expected to levitate at the center of bearings. It is easy to see that equilibrium $(0,0)$ is the only singular point for the corresponding autonomous system of equation (31). The behavior of zero solution depends on the eigenvalues of the corresponding linearized equations (31). There are five cases to be considered:

(1) If $\mu_2 < 0$ and $-\mu_2^2/4 < \mu_1 < 0$, both eigenvalues are real and negative, therefore $(0,0)$ is a stable node.
(2) If $\mu_2 < 0$ and $\mu_1 < -\mu_2^2/4$, both eigenvalues are complex with negative real parts, therefore $(0,0)$ is a stable focus.
(3) If $\mu_2 > 0$ and $\mu_1 < -\mu_2^2/4$, both eigenvalues are complex with positive real parts, therefore $(0,0)$ is an unstable focus.
(4) If $\mu_2 > 0$ and $-\mu_2^2/4 < \mu_1 < 0$, both eigenvalues are real and positive, therefore $(0,0)$ is an unstable node.
(5) If $\mu_1 > 0$, one eigenvalue is positive and the other is negative, therefore $(0,0)$ is a saddle

Figure 6 shows the types of zero solutions of equation (31) in the (μ_1, μ_2)-space. Only in quadrant 3 the zero solution is stable, while in the other quadrants the zero solution is unstable. The higher order terms eliminated in equation (31) do not affect the qualitative behavior of the untruncated system. The dynamics of the original system in the x direction near the fixed point are qualitatively the same as those of the normal form of equation (31).

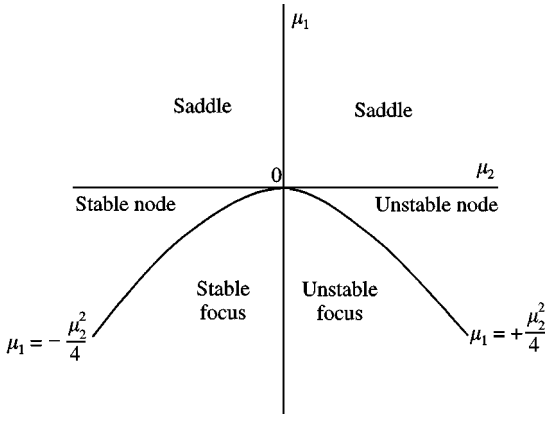

Figure 6. The type of zero solution of equation (33).

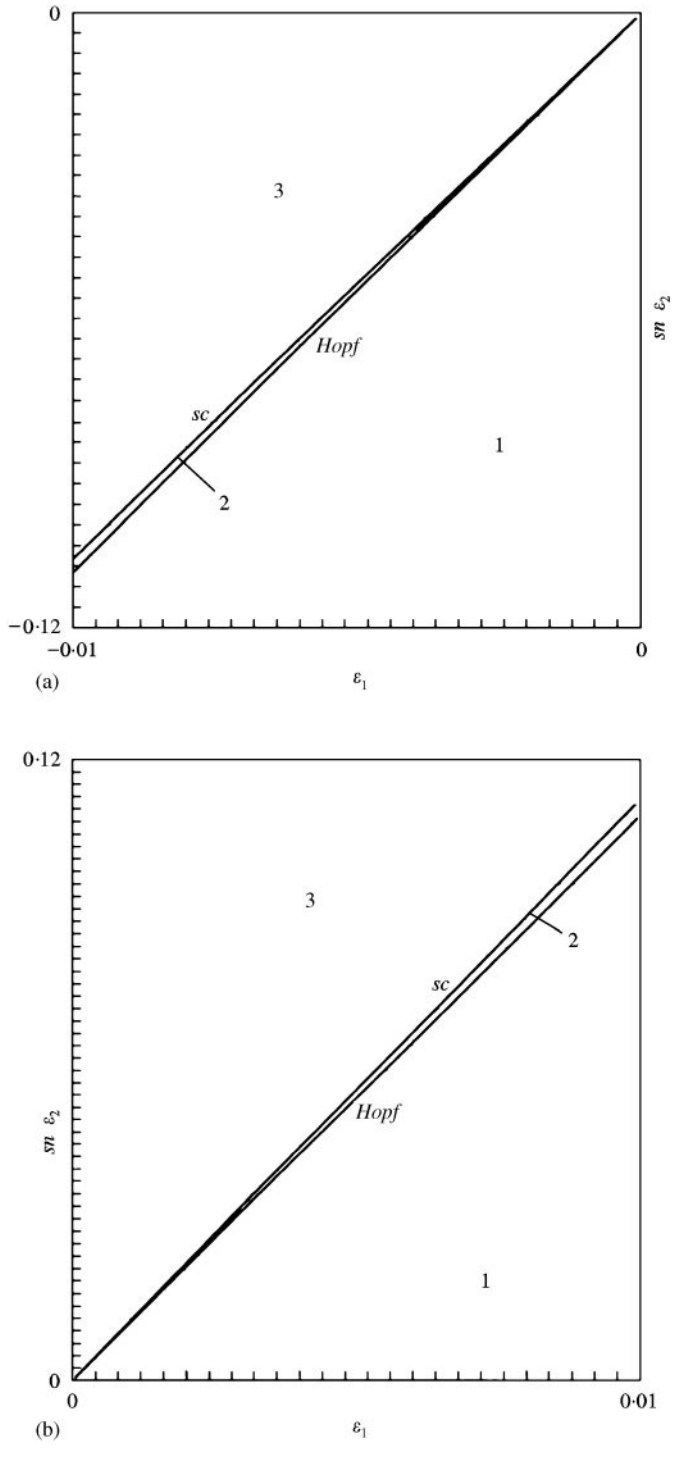

Figure 7. The bifurcation set and phase portraits for autonomous system in the vertical direction. (a) The bifurcation sets in the $(\varepsilon_1, \varepsilon_2)$ plane for the case $\varepsilon_1 \leqslant 0{\cdot}0$ and $\varepsilon_2 \leqslant 0{\cdot}0$. (b) The bifurcation sets for the case $\varepsilon_1 \geqslant 0{\cdot}0$ and $\varepsilon_2 \geqslant 0{\cdot}0$ (c) The phase portrait with $\varepsilon_1 = -0{\cdot}002$ and $\varepsilon_2 = -0{\cdot}022$. (d) The phase portrait with $\varepsilon_1 = -0{\cdot}002$ and $\varepsilon_2 = -0{\cdot}02178$. (e) The phase portrait with $\varepsilon_1 = -0{\cdot}002$ and $\varepsilon_2 = -0{\cdot}02078$. (f) The phase portrait with $\varepsilon_1 = -0{\cdot}002$ and $\varepsilon_2 = -0{\cdot}0148$.

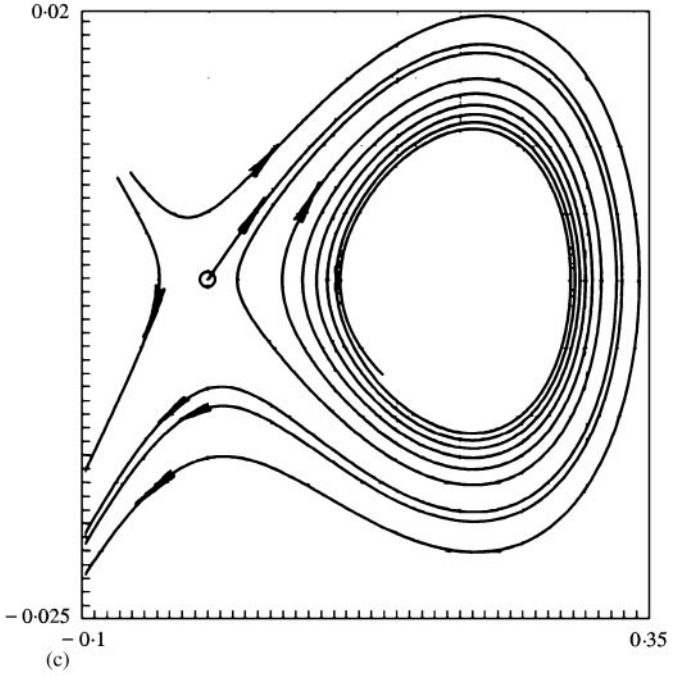

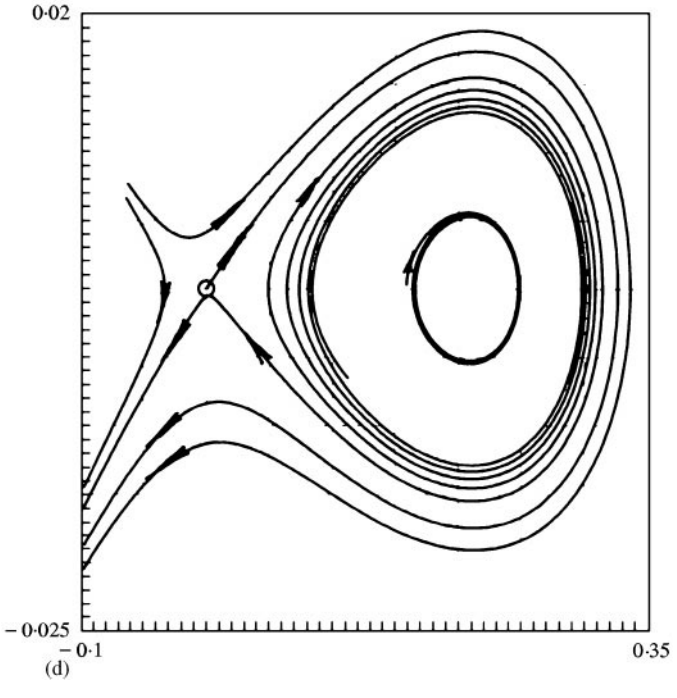

Figure 7. Continued.

6. NUMERICAL SIMULATIONS

In order to verify the above analytical results, the vibratory behavior of the rotor is examined by numerical simulations for double-zero-degenerate case. Direct numerical

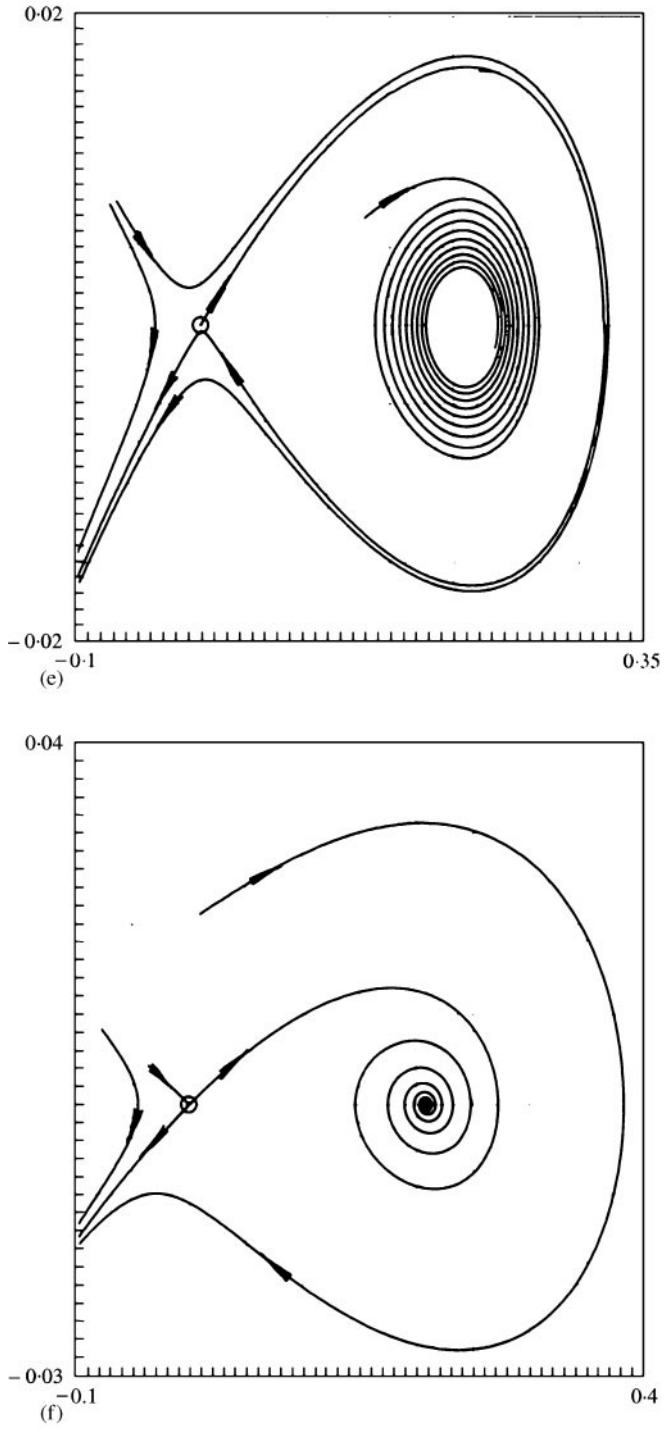

Figure 7. Continued.

simulations were performed for the original system (9) by the Runge–Kutta algorithm. In what follows, $\alpha = 1{\cdot}0$, $w_0 = 0{\cdot}1$, $\delta = 0{\cdot}01$, $\beta = 0{\cdot}1$, $\omega = 1{\cdot}0$. Figure 7 shows the bifurcation sets in the original variables $(\varepsilon_1, \varepsilon_2)$-space and its phase portraits of unforced system in the vertical direction. The bifurcation sets are obtained by translating the analytical results of section 4 back into the original parameter values. Figure 7(a) shows the bifurcation sets for the case $\varepsilon_1 \leqslant 0{\cdot}0$ and $\varepsilon_2 \leqslant 0{\cdot}0$, whereas Figure 7(b) is for the case $\varepsilon_1 \geqslant 0{\cdot}0$ and $\varepsilon_2 \geqslant 0{\cdot}0$. The curves "sn" in Figure 7(a) and 7(b) represent saddle-node bifurcations. The system undergoes a saddle-node bifurcation at $\varepsilon_1 = 0{\cdot}0$. There are a saddle and a source in region 1 (as shown in Figure 7(c)). The circle "○" represent a saddle. The curve "Hopf" represents the Hopf bifurcation and in region 2 (as shown in Figure 7(d)), there are a saddle, a sink, and an unstable limit circle. Upon passing through the Hopf bifurcation curve from region 1, one of the two unstable fixed points becomes stable and an unstable limit circle appears. The periodic orbit created by the subcritical Hopf bifurcation grows in amplitude as ε_2 is increased (or decreased) for the case $\varepsilon_1 \leqslant 0{\cdot}0$ and $\varepsilon_2 \leqslant 0{\cdot}0$ (or $\varepsilon_1 \geqslant 0{\cdot}0$ and $\varepsilon_2 \geqslant 0{\cdot}0$) until it

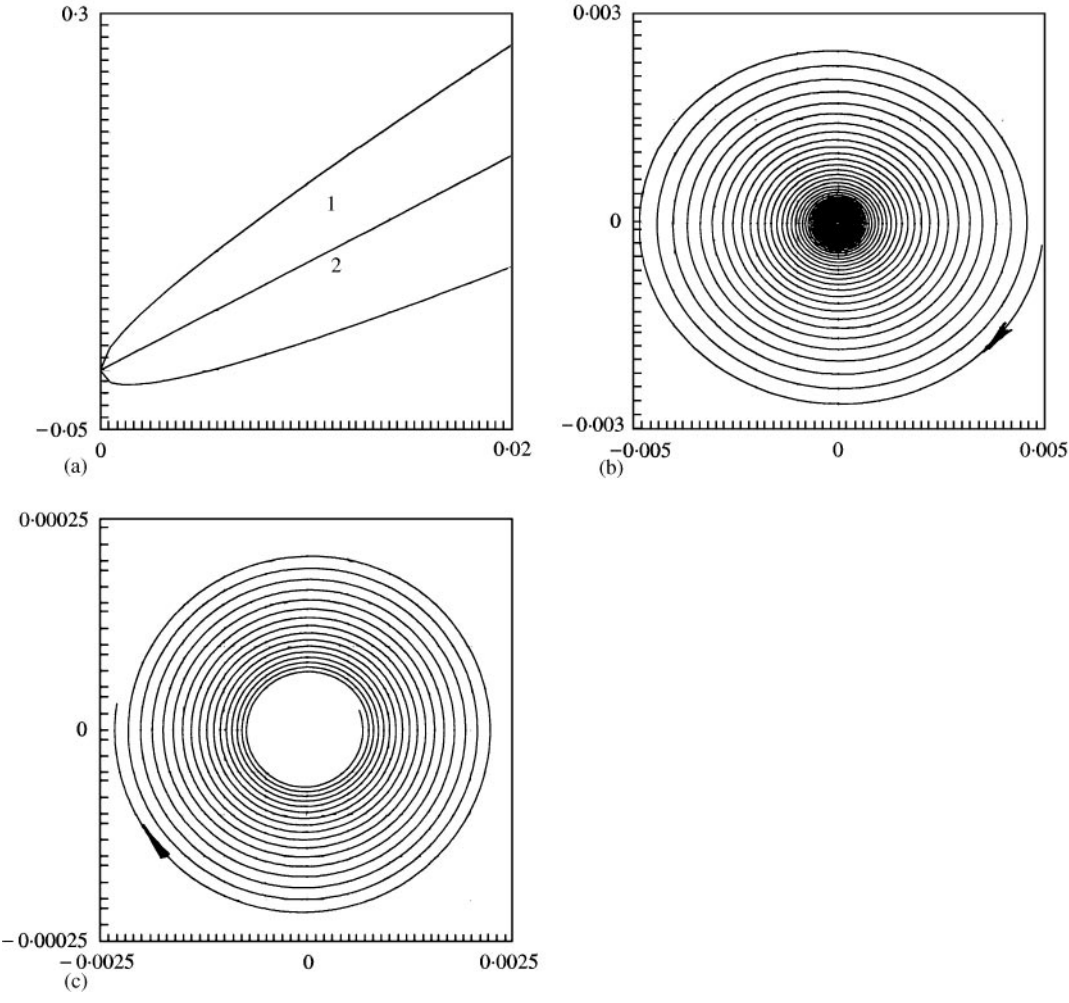

Figure 8. The types of zero solution and partial phase portraits for forced motion in the horizontal direction. (a) Types of zero solution in the $(\varepsilon_1, \varepsilon_2)$ plane, (b) stable focus at $\varepsilon_1 = 0{\cdot}03$ and $\varepsilon_2 = 0{\cdot}282$, (c) unstable focus $\varepsilon_1 = 0{\cdot}005$ and $\varepsilon_2 = 0{\cdot}043$.

collides with the saddle point, creating a homoclinic orbit. The curve "sc" represents a saddle connection or a homoclinic bifurcation (as shown in Figure 7(e)). As ε_2 is further increased (or decreased for $\varepsilon_1 \geqslant 0{\cdot}0$ and $\varepsilon_2 \geqslant 0{\cdot}0$), the homoclinic orbit breaks. In region 3 (as shown in Figure 7(f)), there are a saddle and a sink. Comparing Figures 4 and 7, it is easy to see that the dynamics of original system near the degenerate point are qualitatively the same as those of the truncated normal form. A very good agreement is thus found between the numerical simulations and the analytical results. Figure 8 shows the type of zero solution in the original parameters (ε_1, ε_2)-space and phase portraits for unforced motion in the horizontal direction. Figure 8(b) shows the stable focus associated with region 1, while Figure 8(c) shows the unstable focus corresponding to region 2. A good agreement is also found between analytical results and numerical simulations with comparison between Figures 6 and 8. Figure 9 shows stable periodic orbits of the original system (3) for forced system, which correspond to stable fixed points shown in Figures 4 and 6 respectively.

7. CONCLUSIONS

The dynamics of a rigid rotor suspended by active magnetic bearings are investigated in the neighborhood of the double-degeneracy bifurcation point, by using center manifold theory and normal-form method. These methods can reduce the dynamics to a simpler form while capturing the essentials of dynamical behavior of the original system.

The rotor–AMB system exhibits complicated nonlinear behavior. For the vibrations in the vertical direction, the autonomous system reveals the existence of saddle node, saddle connection and Hopf bifurcations by local bifurcation analyses. The non-autonomous system shows the existence of transversal intersection of the homoclinic orbit by the

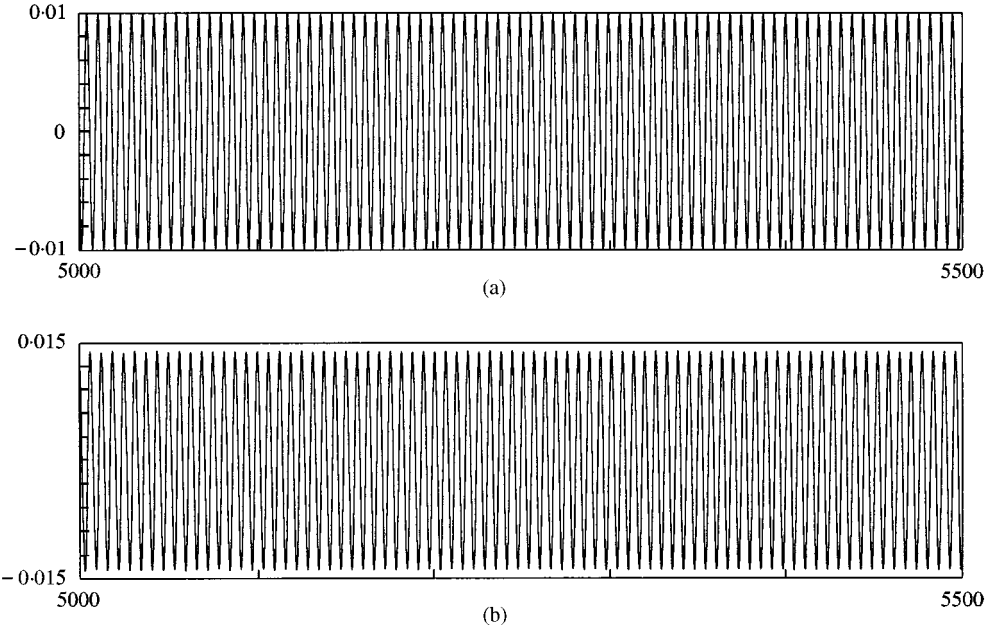

Figure 9. Time histories of stable periodic solutions of the original system (9): (a) The motion in the vertical direction for $f = 0{\cdot}005$, (b) the motion in the horizontal direction for $f = 0{\cdot}01$.

Melnikov analysis. For the vibrations in horizontal directions, the types of zero solution for the autonomous system are discussed. Finally, to verify the analytical results, numerical simulations are performed.

ACKNOWLEDGMENT

This work was supported in part by the National Natural Science Foundation of People's Republic of China and by the City University of Hong Kong.

REFERENCES

1. A. M. MOHAMED and F. P. EMAD 1993 *IEEE Transactions on Automatic Control* **38**, 1242–1245. Nonlinear oscillations in magnetic bearing systems.
2. L. N. VIRGIN, T. F. WALSH and J. D. KNIGHT 1995 *ASME Journal of Engineering for Gas and Turbines and Power* **117**, 582–588. Nonlinear behavior of a magnetic bearing system.
3. M. CHINTA, A. B. PALAZZOLO and A. KASCAK 1996 *Proceedings of 5th International Symposium on Magnetic Bearings*, Kanazawa, Japan, 147–152. Quasiperiodic vibration of a rotor in a magnetic bearing with geometric coupling.
4. M. CHINTA and A. B. PALAZZOLO 1998 *Journal of Sound and Vibration* **214**, 793–803. Stability and bifurcation of rotor motion in a magnetic bearing.
5. P. HOLMES 1985 *ASME Journal of Dynamic Systems, Measurement and Control* **107**, 159–165. Dynamics of a nonlinear oscillator with feedback control I: local analysis.
6. Z. M. GE and H. H. CHEN 1998 *Journal of Sound and Vibration* **209**, 753–769. Double degeneracy and chaos in a rate gyro with feedback control.
7. C. Y. TSENG and P. C. TUNG 1998 *ASME Journal of Vibration and Acoustics* **120**, 39–46. Dynamics of a flexible beam with active nonlinear magnetic force.
8. D. LAIER and R. MARKERT 1995 *Proceedings of the 1st International Conference on Engineering Computation and Computer Simulation ECCS-1, Changsha, China*, Vol. I, 473–482. Simulation of nonlinear effects on magnetically suspended rotors.
9. K. J. HOFFMANN *et al.* 1998 *Proceedings of the 6th International Symposium on Magnetic Bearings, Cambridge, U.S.A.* 256–265. Integrated active magnetic bearings.
10. L. MEIROVITCH 1970 *Method of Analytical Dynamics*. New York: McGraw-Hill.
11. J. GUCKENHEIMER and P. HOLMES 1983 *Nonlinear Oscillations, Dynamical Systems and Bifurcations of Vector Fields*. New York: Springer-Verlag.
12. S. WIGGINS 1990 *Introduction to Applied Nonlinear Dynamical Systems and Chaos*. New York: Springer-Verlag.

APPENDIX A

The non-linear terms, the time-periodic perturbation terms, and the coefficients for equation (12) are shown below:

$$p = \begin{Bmatrix} p_1 \\ p_2 \\ p_3 \end{Bmatrix}, [J] = \begin{bmatrix} 0 & 1 & 0 \\ 0 & 0 & 0 \\ 0 & 0 & -(\delta+\beta) \end{bmatrix}, \quad [J]_\varepsilon = \begin{bmatrix} a_{11} & a_{12} & a_{13} \\ a_{21} & a_{22} & a_{23} \\ a_{31} & a_{32} & a_{33} \end{bmatrix},$$

$$a_{11} = \frac{\alpha_1 + \delta(\delta+\beta)}{(\delta+\beta)^2}\frac{\alpha}{\alpha_1}\varepsilon_1,\ a_{12} = \frac{\alpha_1 + \delta(\delta+\beta)}{\alpha_1(\delta+\beta)^2}\left(\frac{\alpha}{\alpha_1}\delta\varepsilon_1 + \alpha\varepsilon_2\right),$$

$$a_{13} = \frac{\alpha_1 + \delta(\delta+\beta)}{\alpha_1[-\alpha_1 + \beta(\delta+\beta)](\delta+\beta)^2}[-\alpha^2\varepsilon_1 + \alpha^2(\delta+\beta)\varepsilon_2],$$

$$a_{21} = -\frac{\alpha}{(\delta+\beta)}\varepsilon_1,\ a_{22} = -\frac{\alpha}{(\delta+\beta)}\left(\frac{\delta}{\alpha_1}\varepsilon_1 + \varepsilon_2\right),$$

$$a_{23} = \frac{\alpha^2}{(\delta+\beta)(-\alpha_1+\beta(\delta+\beta))}[\varepsilon_1 - (\delta+\beta)\varepsilon_2],\ a_{31} = \frac{-\alpha_1+\beta(\delta+\beta)}{(\delta+\beta)^2}\varepsilon_1,$$

$$a_{32} = \frac{-\alpha_1+\beta(\delta+\beta)}{(\delta+\beta)^2}\left(\frac{\delta}{\alpha_1}\varepsilon_1 + \varepsilon_2\right),\ a_{33} = \frac{1}{(\delta+\beta)^2}[-\alpha_1\varepsilon_1 + \alpha(\delta+\beta)\varepsilon_2].$$

$$T^{-1}\begin{bmatrix}0\\ f(Tp)\\ 0\end{bmatrix} = \frac{-\alpha_1+\beta(\delta+\beta)}{(\delta+\beta)^2}\begin{Bmatrix}-\dfrac{\delta}{\alpha_1}f(Tp)\\ \dfrac{\beta(\delta+\beta)}{-\alpha_1+\beta(\delta+\beta)}f(Tp)\\ \dfrac{\delta}{\alpha}f(Tp)\end{Bmatrix},$$

and

$$T = \begin{bmatrix}1 & \dfrac{\delta}{\alpha_1} & \dfrac{\alpha}{\alpha_1-\beta(\delta+\beta)}\\ 0 & 1 & \dfrac{-\alpha(\delta+\beta)}{\alpha_1-\beta(\delta+\beta)}\\ \dfrac{\alpha_1}{\alpha} & 0 & 1\end{bmatrix}$$

is a matrix composed of generalized eigenvectors of matrix (10).

APPENDIX B

$$C_1 = \frac{\alpha_1-\beta(\delta+\beta)}{(\delta+\beta)^2}\frac{\delta}{\alpha_1},\quad C_2 = \frac{\beta}{\delta+\beta},\quad b_{11} = \frac{\alpha_2}{\alpha}(2\alpha_1-3\alpha),\quad b_{22} = -\frac{3\alpha_2\delta^2}{\alpha_1^2},$$

$$b_{12} = \frac{\alpha_2\delta}{\alpha\alpha_1}(2\alpha_1-6\alpha),\quad b_{111} = -\frac{\alpha_1^2-\alpha\alpha_1}{\alpha},\quad b_{222} = \frac{2\delta^3}{\alpha_1^2},\quad b_{112} = \frac{\alpha_1}{\alpha}\delta,\quad b_{122} = \frac{3\delta^2}{\alpha_1}.$$